



Coupling catalysis and gas phase electrocatalysis for the simultaneous production and separation of pure H₂ and C₂ hydrocarbons from methane and natural gas



A. Caravaca^a, A. de Lucas-Consuegra^{a,*}, V.J. Ferreira^b, J.L. Figueiredo^b, J.L. Faria^b, J.L. Valverde^a, F. Dorado^a

^a Departamento de Ingeniería Química, Facultad de Ciencias y Tecnologías Químicas, Avenida Camilo José Cela 12, 13005 Ciudad Real, Spain

^b LCM – Laboratory of Catalysis and Materials – Associated Laboratory LSRE/LCM, Faculdade de Engenharia, Universidade do Porto, Rua Dr. Roberto Frias s/n, 4200-465, Porto, Portugal

ARTICLE INFO

Article history:

Received 18 March 2013

Received in revised form 29 April 2013

Accepted 8 May 2013

Available online 15 May 2013

Keywords:

Gas-phase electrocatalysis

Pure H₂ production

Oxidative coupling

Steam electrolysis

C₂ hydrocarbons

ABSTRACT

This study reports the simultaneous production of pure H₂ and C₂ hydrocarbons (ethane and ethylene) in a solid oxide electrolysis cell coupled with an active catalyst powder bed. For first time, an Ag/YSZ/Ag double chamber cell was used and high yields to both, hydrogen and C₂ hydrocarbons were achieved. The separately feeding of H₂O and CH₄ to the inner and outer chamber of the reactor, respectively, allows to obtain both kinds of products streams. Thus, steam was electrolyzed on the inner Ag electrode of the electrochemical cell (cathode), producing pure H₂ (as the first product) and O^{2−} ions, which were electrochemically supplied through the YSZ solid electrolyte to the outer Ag electrode (anode). On this latter, the reaction of the O^{2−} ions and the oxygen evolved with the methane stream led to the production of C₂ hydrocarbons (together with CO and CO₂ as secondary combustion products). The C_{2s} yield of this outer stream was strongly enhanced by the addition of an active catalyst powder bed (Ce–Na₂WO₄/SiO₂ or Mn–Ce–Na₂WO₄/SiO₂) to obtain the second product stream (with a high C₂ yield up to 15%). The influence of the oxidative coupling catalyst powder bed, the reaction temperature and the gas phase composition was studied. Finally, the optimized system was studied by feeding a synthetic natural gas stream (instead of CH₄) in order to approach to a more practical system. The high performance of the system was again verified along with a durability test under polarization conditions in view of the possible practical application of this novel reactor configuration system.

© 2013 Elsevier B.V. All rights reserved.

1. Introduction

In the recent years, there is an increasing demand for ethylene in both developed and developing countries. Ethylene has a large market and is the most produced organic compound in the world [1]. It is conventionally produced in the petrochemical industries by steam cracking of different liquid feedstock, especially naphtha. However, since the work carried out by Keller and Bhasin [2], much attention has been paid to the catalytic methane oxidative coupling process for the production of C₂ hydrocarbons (mainly ethylene). In this sense, the use of solid electrolyte membrane reactors has been demonstrated to be a suitable and promising technology for the production of these compounds via catalytic oxidative coupling process [3–8]. The option of using this kind of reactors presents

several advantages such as: enhanced catalytic activity and selectivity, better process integration, reduced feedstock and easy reaction rate control. This kind of systems allows to perform oxidation and partial oxidation reactions (methane coupling) without feeding pure O₂ to the reactor atmosphere (by an in situ steam electrolysis process). Hence, the use of this kind of reactor configurations allows the simultaneous production of H₂ along with the C₂ hydrocarbons [3,4,7,8] by coupling a steam electrolysis process. However, in most of these previous works, low yields of C₂ hydrocarbons were obtained, mainly due to the low catalytic activity and surface area of the used electrodes. In this sense, in a previous work carried out by our group [8], we demonstrated the possibility of increasing the C_{2s} yield in a single chamber solid electrolyte membrane reactor by the addition of an active catalyst powder. This previous study also demonstrated the lower electrical energy requirements of the solid electrochemical membrane reactor to produce the same amount of H₂ and C_{2s} hydrocarbons when adding the active catalyst powder bed. Nevertheless, low

* Corresponding author. Tel.: +34 926 295300; fax: +34 926 295437.

E-mail address: Antonio.Lconsuegra@uclm.es (A. de Lucas-Consuegra).

faradaic efficiency values were still obtained for H_2 production (around 25%) associated with the non-desired reaction of H_2 with the other products (CO_2 and O_2) in the single chamber atmosphere cell. In addition, H_2 and the other products (CO , CO_2 , O_2 and C_2 hydrocarbons) were mixed in a unique product stream. Therefore, further separation steps should be required for the valorization of the desired products.

In this work we propose a novel reactor configuration, which combines catalysis and gas phase electrocatalysis, for the simultaneous production and separation of a completely pure H_2 stream and a C_{2s} hydrocarbons rich one (with a high yield). For this purpose, we have developed a Ag/YSZ/Ag double chamber steam electrolysis cell coupled with an active oxidative coupling catalyst bed (Ce– Na_2WO_4/SiO_2 or Mn–Ce– Na_2WO_4/SiO_2). These catalysts have been reported to be active in the oxidative coupling of methane [1,9] which would allow to strongly increase the C_{2s} yield of the hydrocarbon rich stream. Thus, the influence of the oxidative coupling catalyst powder bed, the reaction temperature and the gas phase composition was studied. Finally, the optimized system was analyzed by feeding a synthetic natural gas stream (instead of CH_4) in order to approach the system to a more practical one. A high performance was again verified, along with a durability test under polarization, which demonstrated the stability of all the components of the system: the solid electrolyte, the Ag electrodes and the catalyst powder bed.

2. Experimental

2.1. Preparation and characterization of the catalyst powders

Two kind of SiO_2 supported catalyst powders were synthesized and characterized in this work: Ce– Na_2WO_4/SiO_2 and Mn–Ce– Na_2WO_4/SiO_2 . Briefly, the silica catalyst support was synthesized following a procedure similar to that reported by Wang et al. [10]. A mixture of H_2O , ethanol and tetraethylorthosilicate (99% Aldrich TEOS) was prepared and mixed with an NH_4OH aqueous solution containing 0.16 g of citric acid under stirring until a gel was obtained. The precipitated obtained was washed with distilled water and dried in an oven at $120^\circ C$. Finally, the product was calcined at $500^\circ C$ for 2 h to obtain the silica material. Then, the active catalyst powders were prepared by incipient wetness impregnation of the synthesized silica support with aqueous solutions of the precursors. Cerium, manganese and sodium tungsten impregnations to prepare the 5 wt%Ce–5 wt% Na_2WO_4/SiO_2 and 5 wt%Ce–5 wt%Mn–5 wt% Na_2WO_4/SiO_2 catalysts were performed using aqueous solutions of $Ce(NO_3)_3 \cdot 6H_2O$ (99% Aldrich), $Mn(NO_3)_2 \cdot 4H_2O$ (97% Sigma–Aldrich) and $Na_2WO_4 \cdot 2H_2O$ (99% Riedel–deHaën) with the appropriate concentration. Impregnated catalysts were dried at $120^\circ C$ after each impregnation overnight, followed by calcination at $800^\circ C$ during 8 h.

Regarding the characterization of the catalyst powders, BET surface areas of the samples were measured from the corresponding N_2 equilibrium adsorption isotherms, determined at $-196^\circ C$ with a Quantachrome Instruments NOVA 4200e apparatus. X-ray diffraction analyses of fresh and used catalyst powders were carried out on a Philips PW 1710 instrument using Ni-filtered Cu K α radiation.

2.2. Combined solid electrolyte cell-fixed bed reactor

The solid electrolyte cell consisted on an yttria-stabilized zirconia (YSZ) tube closed at one end, with 15 cm length, 1.8 cm internal diameter, and 1.5 mm thickness (supplied by CERECO). On both faces of the closed side tube (Fig. 1), two Ag porous electrodes were prepared by application of thin coatings of Ag paste (fuel cell materials), followed by two calcination steps, at $300^\circ C$

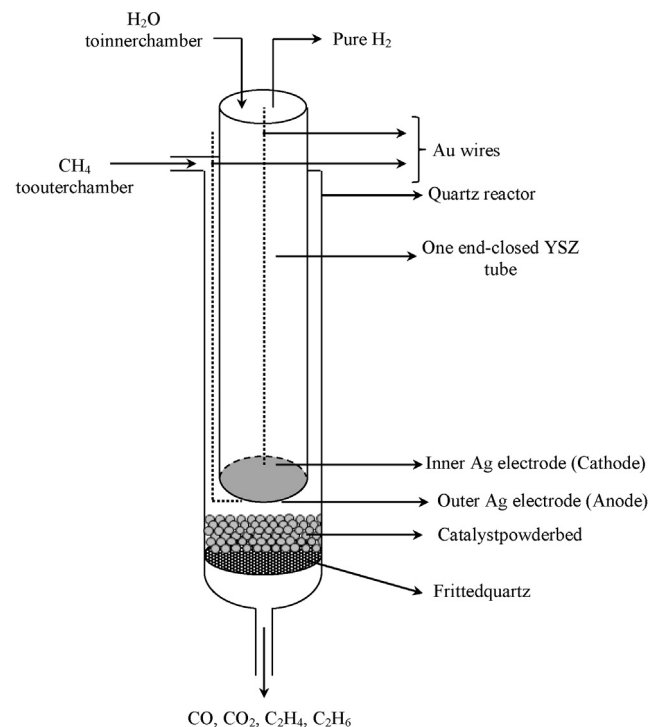


Fig. 1. Scheme of the double chamber solid electrolyte cell reactor.

(2 h) and $850^\circ C$ (2 h). The final Ag loading of each electrode was around 10 mg Ag/cm^2 . The electrical contact of both electrodes was carried out by gold wires, which were in turn connected to a potentiostat–galvanostat Voltalab 21 (Radiometer Analytical). Hence, the inner Ag electrode acted as a working electrode and as a cathode, while the outer Ag layer acted as a counter electrode and as anode of the solid electrolyte cell. In this work, all the experiments were carried out under galvanostatic imposition mode. The reaction experiments were carried out in a double chamber solid oxide electrolysis cell coupled with a catalyst powder bed, as shown in Fig. 1. The cell reactor was made of a quartz tube with appropriate feed-through and incorporates an inner fritted quartz. Firstly, 200 mg of the powder catalyst (Ce– Na_2WO_4/SiO_2 or Mn–Ce– Na_2WO_4/SiO_2) were placed on the fritted quartz (22 mm in diameter). Then, the solid electrolyte cell was placed above the catalyst bed (at around 5 mm). The inner Ag working electrode (W) was exposed to a H_2O/N_2 mixture, whereas the outer face, the Ag counter electrode (C), was exposed to a CH_4/N_2 or natural gas/ N_2 feed stream. Hence, both reactions atmospheres were completely isolated. No gas permeation occurred between the two chambers, as verified by blank H_2 leak measurements.

2.3. Catalytic activity measurements

The reaction gases (Praxair, Inc.) were certified standards of 10% CH_4/N_2 , natural gas, and N_2 (99.999% purity) used as carrier gas. The gas flow was controlled by a set of calibrated mass flowmeters (Brooks 5850 E and 5850 S) while water was introduced into the feed stream by means of a saturator in order to achieve liquid–vapor equilibrium. Then, water was introduced in the inner chamber. Its content was controlled by the vapor pressure of H_2O at the temperature of the saturator ($45^\circ C$). Thus, 10% water was introduced in a 50 mL min^{-1} feed stream. All lines placed downstream from the saturator were heated above $100^\circ C$ to prevent condensation. Regarding the outer chamber, the reactants were introduced with the following concentrations: CH_4 (0.2–1.5%) or natural gas (10%), N_2 (balance), with an overall gas flow rate of $50 \text{ cm}^3 \text{ min}^{-1}$. It led to

Table 1
Molar composition of the synthetic natural gas.

	Molecular formula	Concentration (%)
N-Butane	C ₄ H ₁₀	0.30
Isobutane	C ₄ H ₁₀	0.30
Propane	C ₃ H ₈	1.49
Ethane	C ₂ H ₆	4.94
Methane	CH ₄	92.96

Table 2
BET surface area and pore volume of the silica support, and the Ce–Na₂WO₄/SiO₂ and Mn–Ce–Na₂WO₄/SiO₂ powder catalysts.

	Surface area (m ² g ^{−1})	Pore volume (mL g ^{−1})
SiO ₂	15	5.1 × 10 ^{−2}
5 wt%Ce–5 wt%Na ₂ WO ₄ /SiO ₂	9.3	1.2 × 10 ^{−3}
5 wt%Ce–5 wt%Mn–5 wt%Na ₂ WO ₄ /SiO ₂	2.7	8.0 × 10 ^{−4}

a gas hourly space velocity (GHSV) of 15,000 cm³ g^{−1} h^{−1} respect to the catalyst powder bed. All the catalytic experiments were carried out at atmospheric pressure and at reaction temperatures between 750 and 800 °C. For the case of the experiments with the synthetic natural gas, the composition of the inlet stream is shown in Table 1. Hydrogen produced in the inner chamber was calculated on the basis of the Faraday's law. Reactant and product gases of the outer chamber were analyzed with a micro gas-chromatograph (Varian CP-4900) equipped with two columns (Molsieve and Poraplot Q column) and two thermal conductivity detectors (TCD). The main detectable products of the outer side stream were C₂H₆, C₂H₄, CO₂, CO and H₂. The deviation associated to the carbon balance did not exceed 1% in the whole study, which indicated no significant formation of other oxygenated species and/or coking of the catalyst-electrodes. It was further confirmed by the high stability of the present system for long operation times. CH₄ conversion, C_{2s} selectivity and C_{2s} yield were calculated by the following equations [7,8]:

$$\text{CH}_4 \text{ conversion} = \frac{F_{\text{CH}_4}^0 - F_{\text{CH}_4}^{\text{out}}}{F_{\text{CH}_4}^0} \times 100 \quad (1)$$

$$\text{C}_{2s} \text{ selectivity} = 2 \times \left(\frac{F_{\text{C}_2\text{H}_4} + F_{\text{C}_2\text{H}_6}}{F_{\text{CH}_4}^0 - F_{\text{CH}_4}^{\text{out}}} \right) \times 100 \quad (2)$$

$$\text{C}_{2s} \text{ yield} = \frac{\text{CH}_4 \text{ conversion} \times \text{C}_{2s} \text{ selectivity}}{100} \quad (3)$$

3. Results and discussion

3.1. Characterization of the 5 wt%Ce–5 wt%Na₂WO₄/SiO₂ and 5 wt%Ce–5 wt%Mn–5 wt%Na₂WO₄/SiO₂ catalyst powders

BET surface area and pore volume of the silica support were measured to be 15.0 m² g^{−1} and 0.051 mL g^{−1}, respectively. Data corresponding to catalysts 5 wt%Ce–5 wt%Na₂WO₄/SiO₂ and 5 wt%Ce–5 wt%Mn–5 wt%Na₂WO₄/SiO₂ are shown in Table 2. The obtained results depict a reduction of the textural parameters of both catalysts in comparison with those of the silica support. It would indicate the crystallization of amorphous silica, making the materials almost nonporous [1].

XRD spectra of fresh catalysts 5 wt%Ce–5 wt%Na₂WO₄/SiO₂ and 5 wt%Ce–5 wt%Mn–5 wt%Na₂WO₄/SiO₂ are shown in Fig. 2a and b. For both catalysts, it can be observed the presence at 22° of a peak corresponding to the presence of α-cristobalite. It is well known that the transformation of amorphous silica to highly crystalline α-cristobalite occurs in the presence of an alkali like

sodium tungstate acting as the mineralizing agent [11]. CeO₂ and Na₂WO₄ phases were also identified in both catalysts. In addition, the presence of crystalline Mn₂O₃ was observed in catalyst 5 wt%Ce–5 wt%Mn–5 wt%Na₂WO₄/SiO₂. A strong difference of the crystallinity of both catalyst powders can be observed in this figure. Thus, the crystallinity of the Mn doped catalyst was higher than that for catalyst Ce–Na₂WO₄/SiO₂ (the peak at 22° in the Mn doped catalyst diffractogram shows a higher intensity). In a previous study [12], Ce has been reported to act as a crystallization inhibitor. Moreover, the BET measurements shown in Table 2 depicted a stronger reduction of the structural parameters for the Mn doped catalyst. It suggests that Mn have a significant effect on the structural properties, inducing the crystallization of the amorphous silica support.

Similar catalyst powders have been reported in literature to be active in the methane oxidative coupling process [1,8,9,13]. For instance, ceria is known to be an oxygen activator with high oxygen storage capacity [1] whereas the Mn doped Na₂WO₄ catalyst system, firstly reported by Fang et al. [14], attracted great attention because of its outstanding catalytic performance. Thus, they have been widely studied in previous works [9,13,15–17]. Consequently, these materials were selected to use together with the solid electrolyte membrane reactor for the electro-catalytic experiments described in the next section.

3.2. Electro-catalytic experiments with methane

Firstly, a dynamic galvanostatic transient experiment was carried out at a constant temperature of 750 °C. It was performed under current imposition step changes between −10 and −45 mA by passing the following streams: 1% CH₄ for the outer chamber and 10% H₂O for the inner chamber, both of them balanced with N₂ at a total flow rate of 50 mL min^{−1}. Fig. 3a (left) depicts the variation of the obtained products reaction rates with the time on stream under different current impositions, and Fig. 3b represents the scheme of the different reactions and process that occurred on the system. The dense box simulates the separation between the inner and the outer chamber. It should be mentioned that for all the studied systems, the activity under open circuit conditions (not shown here), i.e., at current = 0 mA, was negligible due to the absence of any oxygen electrochemically supplied to the outer chamber. Hence, methane catalytic decomposition activity was not provided neither by the Ag electrodes nor by the active catalyst powder materials at the explored temperature range. Moreover, the open circuit potential was close to 0 V, neglecting therefore the possibility of spontaneous steam electrolysis in the inner chamber. On the other hand, it could be observed that an increase in the applied current led to a strong increase in the production rate for all the products. It could be easily understood with the scheme shown in Fig. 3b.

The YSZ solid electrolyte could be considered as a pure O^{2−} conductor. Thus, the application of negative currents (being the inner Ag electrode the working and the outer Ag electrode the counter) led to the steam electrolysis process in the Ag inner electrode, which led to the production of pure gaseous H₂, and O^{2−} ions [7,8]. Hence, the H₂ production rate in the inner chamber could be calculated on the basis of the Faraday's law by 1/2 *F*, where *I* is the applied current, and *F* is the Faraday's constant. Then, an increase of the applied current led to a proportional increase of both the pure hydrogen produced and the amount of electrochemically pumped O^{2−} ions from the inner to the outer Ag electrode. It led to the production of carbon derived products according to the global reactions depicted in Fig. 3b. Regarding the solid electrolyte cell (SEC from now on), these O^{2−} ions could directly react in the Ag outer electrode with methane (reaction 1) to produce a mixture of C_{2s} and CO_x [7,8]. Moreover, as proposed by Tsiakaras and Vayenas [18], the formation of oxygen dissolved species could activate the Ag catalyst to form ethane. Then, it would react with

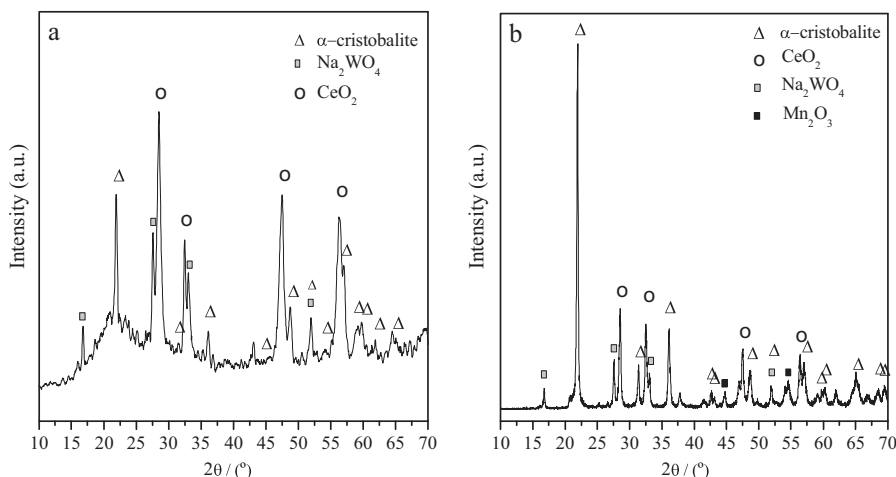


Fig. 2. XRD pattern of the fresh catalysts 5 wt%Ce–5 wt%Na₂WO₄/SiO₂ (a) and the 5 wt%Mn–5 wt%Ce–5 wt%Na₂WO₄/SiO₂ (b).

the oxygen evolved to the gas phase (reaction 3) to form ethylene and CO₂ (reaction 2). However, as it could be observed in Fig. 3a, the production rate of oxidative coupling (C₂⁺ hydrocarbons) and combustion (CO_x) products was practically negligible (but not null) in the SEC system in comparison with the reaction rate of these compounds under the presence of the active catalyst powder bed in the outer chamber (SEC+PC system from now on). It could be attributed, for instance, to the low applied currents (45 mA), which limited the catalytic/electrocatalytic activity of the Ag electrode and, on the other hand, to the reaction of the free oxygen evolved to the gas phase (reaction 3) with methane in the catalyst bed,

strongly increasing the catalytic activity of the system (reactions 4–7). Hence, an increase of the applied current, with the concomitant increase in the O₂ pumping rate from the inner to the outer chamber, led to an increase of methane conversion via oxidative coupling (reactions 4 and 5), total oxidation (reaction 6) and partial oxidation (reaction 7), increasing the production rate of C₂s, CO_x (CO + CO₂) and H₂. Concerning the C₂s production, both catalysts provided a fairly similar activity for the methane coupling reaction at the explored temperature. However, the Ce–Na₂WO₄/SiO₂ showed higher H₂ and CO_x production rates, due to the superior performance of this material for the total and partial oxidation

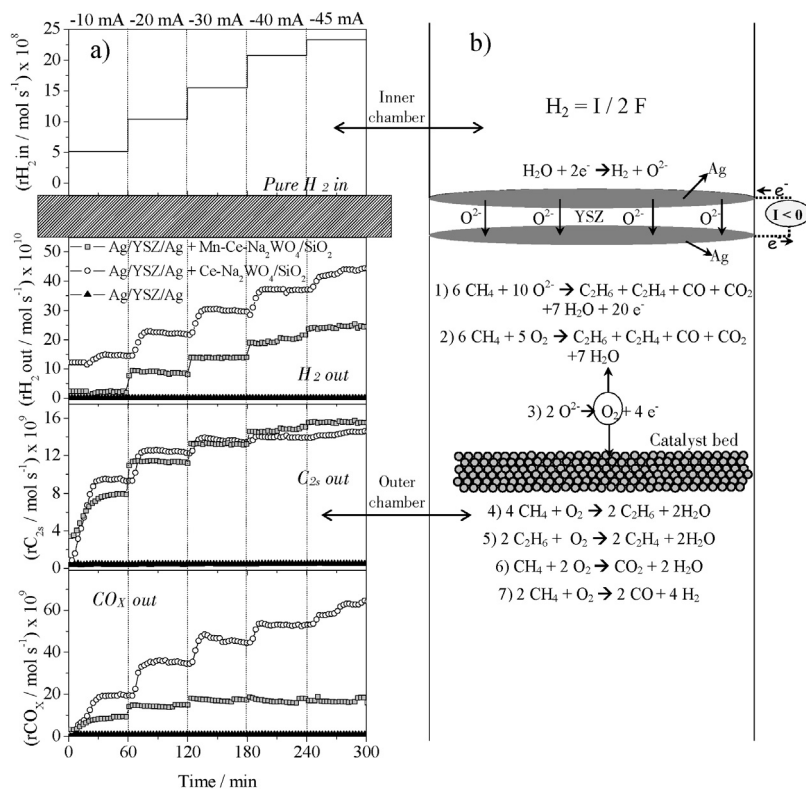


Fig. 3. Influence of the applied current on the dynamic value of the inner (pure H₂) and the outer chamber products (H₂, C₂s and CO_x) for the Ag/YSZ/Ag, Ag/YSZ/Ag+Ce–Na₂WO₄/SiO₂ and Ag/YSZ/Ag+Mn–Ce–Na₂WO₄/SiO₂ systems (a). Schematic representation of the main processes involved during the cathodic polarizations for the above-mentioned systems (b). Conditions: outer chamber CH₄=1%, inner chamber H₂O=10%, total flow in both chambers=50 cm³ min⁻¹ (N₂ balance), temperature=750 °C.

methane activity. Despite, at any case, the H_2 production rate in the outer chamber via partial oxidation was around two magnitude order lower than the H_2 produced via electrolysis in the inner chamber.

In a previous study with a single chamber configuration [8], it was demonstrated that the SEC performance can be improved for H_2 and C_2 hydrocarbons production by the introduction of a catalyst $Ce-Na_2WO_4/SiO_2$ powder. However, the experiment shown in Fig. 3a demonstrates, for the first time in literature, the possibility of simultaneously producing and separating hydrogen and C_2 hydrocarbons with a YSZ-based solid electrolyte cell. Moreover, as it will be shown in the following experiments, high C_{2s} yields (up to 15%) can be obtained with an electro-catalytic system based on a tubular YSZ solid electrolyte cell coupled with a powder catalyst bed. In this sense, other electro-catalytic and membrane based systems have been used in literature for the simultaneous production/separation of H_2 and C_{2s} [3,4,19]. For instance, the studies carried out by the group of Stoukides have demonstrated this concept with solid electrolyte proton conductors [3,4]. However, low current densities (accompanied with a low hydrogen production) and low C_{2s} yield were obtained with this configuration. Moreover, a recent study carried out by Cao et al. [19] used a similar system as that proposed in this work. It consisted of a double chamber configuration separated by a BSCF oxygen-permeable membrane and coupled with a Mn doped Na_2WO_5/SiO_2 powder catalyst. In that study, the oxygen produced in the inner chamber from thermal water splitting was transported through the BSCF membrane, being consumed in the methane oxidative coupling process occurring in the catalyst bed placed in the outer chamber. However, the results obtained revealed lower C_{2s} yields compared to those reported in this work. Moreover, some important advantages could be highlighted for the system used in our study vs. the previous work [19], such as lower operation temperature ($800^\circ C$ vs. $950^\circ C$) as well as an electrical control of the product reaction rates (H_2 and C_{2s}). Moreover, water splitting at high temperatures is a thermodynamically controlled reaction, and hence only small amounts of hydrogen can be generated at equilibrium due to the very low equilibrium constant [20].

Next, the influence of the reaction temperature on the performance of the system was studied. In order to fix the working

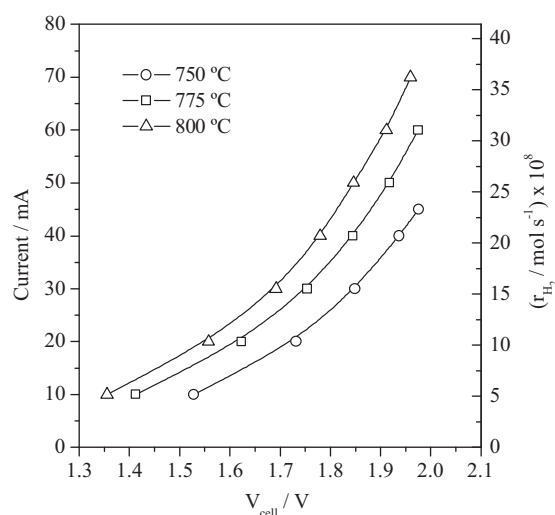


Fig. 4. Influence of the reaction temperature on both the polarization curves and the H_2 production for the Ag/YSZ/Ag solid electrolyte cell.

potential range of the cell, the steady state current–potential curves (in absolute values) of the solid electrolyte cell were obtained at three different operation temperatures (750, 775 and $800^\circ C$) under the same feed stream conditions of the previous experiment (1% CH_4 in the outer chamber, and 10% H_2O in the inner chamber). The polarization curves were performed until a maximum cell potential of 2 V in order to preserve the stability and avoid the reduction of the YSZ solid electrolyte. Thus, maximum currents of -45 , -60 and -70 mA were obtained at 750, 775 and $800^\circ C$, respectively, at a cell potential close to -2 V (Fig. 4). In addition, the secondary Y-axis shows the equivalent pure H_2 production rate obtained in the inner chamber (calculated via Faraday's law) for each polarization. It could be observed that no mass transfer limitations occurred at any temperature, since no limiting current at the studied potential range was observed [21]. Moreover, as expected, a reaction temperature increase led to a current increase at a fixed cell potential and, consequently, to a higher H_2 production rate. It could be attributed

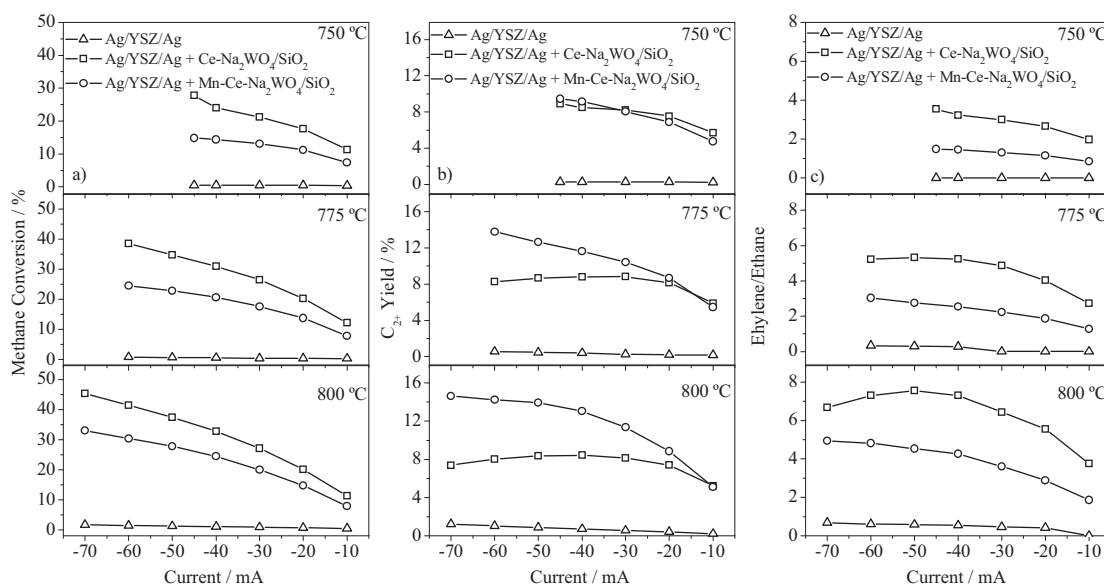


Fig. 5. Influence of the reaction temperature and the current imposition for the Ag/YSZ/Ag, Ag/YSZ/Ag + $Ce-Na_2WO_4/SiO_2$ and Ag/YSZ/Ag + $Mn-Ce-Na_2WO_4/SiO_2$ systems on: (a) CH_4 conversion, (b) C_{2s} yield and (c) C_2H_4/C_2H_6 ratio. Conditions: outer chamber $CH_4 = 1\%$, inner chamber $H_2O = 10\%$, total flow in both chambers = $50\text{ cm}^3\text{ min}^{-1}$ (N_2 balance), temperature = $750\text{--}800^\circ C$.

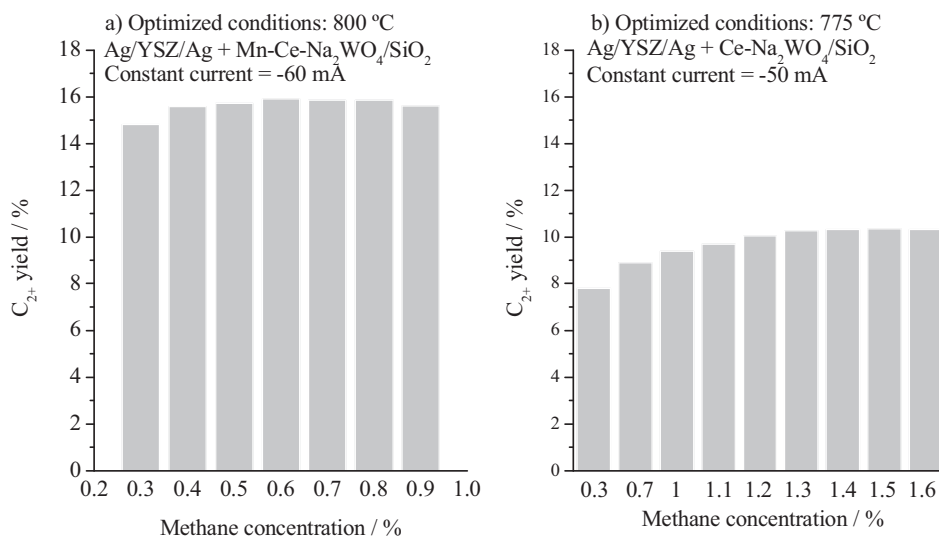


Fig. 6. Influence of the inlet CH₄ concentration under fixed current imposition on the C_{2s} yield for the Ag/YSZ/Ag + Ce-Na₂WO₄/SiO₂ and Ag/YSZ/Ag + Mn-Ce-Na₂WO₄/SiO₂ systems. Conditions: outer chamber CH₄ = 0.3–1.6%, inner chamber H₂O = 10%, total flow in both chambers = 50 cm³ min⁻¹ (N₂ balance), temperature = 775 and 800 °C.

to an enhancement of the reaction rate for the steam electrolysis process and the increase of the O²⁻ ionic conductivity of the YSZ solid electrolyte.

Fig. 5 depicts the influence of the reaction temperature on the main reaction parameters of the oxidative coupling process at the outer chamber for the SEC and the SEC + PC systems: methane conversion (Fig. 5a), C_{2s} yield (Fig. 5b) and ethylene/ethane ratio (Fig. 5c). Feed stream compositions were the same as described for previous experiments. The explored current application range at each temperature was selected according to the previously obtained current–potential curves. In first place, it can be observed that the methane conversion over the outer Ag electrode was almost negligible at all the explored reaction temperatures. Then, the activity was mainly provided by the addition of the catalyst powders, in good agreement with the experiments shown in Fig. 3. It can be also observed a higher methane conversion under the presence of the Ce-Na₂WO₄/SiO₂ catalyst (Fig. 5a). However, higher activity toward methane oxidative coupling process was observed for the Mn doped catalyst (higher C_{2s} yield, as observed in Fig. 5b). This latter can be clearly observed at temperatures higher than 750 °C, where similar C_{2s} production rates were detected for both catalysts (Fig. 3). This higher activity could be explained according to the higher crystallinity observed for the Mn doped catalyst (Fig. 2). Previous works have demonstrated that the phase transition from amorphous silica to crystalline form (α-cristobalite) is an essential requirement for an effective oxidative coupling catalyst [1]. According to the work performed by Palermo et al. [22], amorphous silica could be identified by a wide peak (2θ = 15–25°), which follows a similar trend as the base line of the diffractogram shown in Fig. 2a for catalyst Ce-Na₂WO₄/SiO₂. It is in good agreement with the lower crystallinity of this catalyst compared to that of the Mn-Ce-Na₂WO₄/SiO₂ catalyst. It seems to be that part of the amorphous SiO₂ support did not crystallize into α-cristobalite during the calcination process. In this sense, Arndt et al. [13] reported that amorphous SiO₂, with and without Na, is basically a total oxidation catalyst. After the phase transition to α-cristobalite, the material can be considered as inert. It supports, as mentioned in Fig. 5a and b, the higher activity of catalyst Ce-Na₂WO₄/SiO₂ toward methane combustion. Moreover, Palermo et al. [22] reported that strong synergies are present between Mn, W and Na metal oxides, which would enhance the oxidative coupling mechanism. Finally, it should be mentioned that the Mn doped Ce-Na₂WO₄/SiO₂ catalyst has been previously used in literature [9], showing

a good performance toward the catalytic oxidative coupling process.

Fig. 5c depicts the variation of the ethylene/ethane ratio under the different conditions studied. For both SEC + PC systems, the increase of the reaction temperature and the applied current had a positive effect on this ratio. Moreover, the obtained values for both systems were relatively high (ethylene/ethane > 4) for most of the explored currents, if they are compared to those obtained in similar studies reported in the literature for ethylene/ethane ratios ranging from 2 to 3 [1,9]. It could be attributed to the homogeneous oxidative dehydrogenation of ethane (ODE) reached with our reactor configuration. As reported in literature [23–25], an important activity for the non-catalytic or homogeneous ODE reaction could be found in the reaction temperature range studied in this work. In addition, catalyst Ce-Na₂WO₄/SiO₂ led to a higher ethylene/ethane ratio. Taking into account the O₂ balance, the oxygen conversion was enhanced over this catalyst bed. As reported by Choudhary and Mulla [24], an increase of the oxygen present in the reaction atmosphere led to a lower selectivity toward ethylene in benefit of the CO_x one, which would be a consequence of the occurrence of the homogeneous oxidation of ethane. It would explain the lower ethylene/ethane ratio obtained by the Mn doped catalyst. Nevertheless, the ethylene yield for this latter catalyst was higher under all the explored conditions, which would again demonstrate the better performance of the Ag/YSZ/Ag + Mn-Ce-Na₂WO₄/SiO₂ system.

The maximum C₂₊ yield for catalyst Ce-Na₂WO₄/SiO₂ was found at 775 °C (higher temperatures enhanced the methane combustion in detriment of the oxidative coupling process), while for catalyst Mn-Ce-Na₂WO₄/SiO₂ the maximum C₂₊ yield occurred at 800 °C. Hence, in order to optimize the reaction parameters as a function of the composition, the methane concentration was changed considering a fixed oxygen partial pressure under a constant current application and the same feed stream conditions in the inlet chamber (10% H₂O, 50 mL min⁻¹, N₂ balance), at the aforementioned temperatures. Fig. 6 shows the C₂₊ yields obtained for the SEC + PC system with the different catalysts powders at the different methane concentrations. As observed, the production of C₂₊ passed through a maximum for both systems. Based on the reaction products, the optimum could be explained attending to the competition between the methane coupling and combustion processes. Thus, although the overall methane reaction rate increased with the methane concentration, the selectivity toward C_{2s} hydrocarbons decreased, leading to an optimum C_{2s} yield. On the other

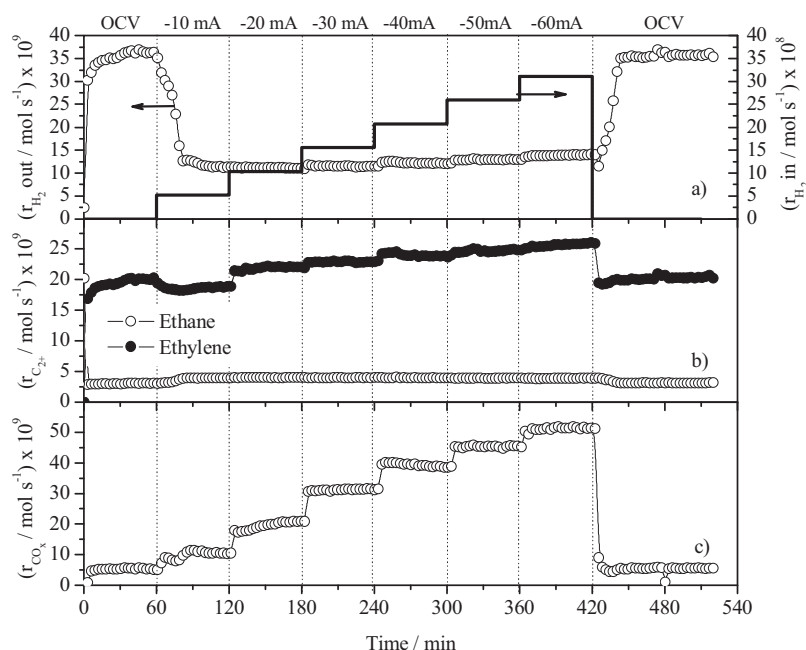


Fig. 7. Influence of the applied current on the dynamic value of the outer chamber products (H_2 , C_2H_6 , C_2H_4 , and CO_x) for the $\text{Ag}/\text{YSZ}/\text{Ag} + \text{Mn}-\text{Ce}-\text{Na}_2\text{WO}_4/\text{SiO}_2$ system. Conditions: outer chamber natural gas = 1%, inner chamber H_2O = 10%, total flow in both chambers = $50 \text{ cm}^3 \text{ min}^{-1}$ (N_2 balance), temperature = 800°C .

hand, it should be mentioned that the CH_4/O_2 ratio that optimizes the $\text{C}_{2\text{s}}$ yield for the SEC system coupled with the $\text{Ce}-\text{Na}_2\text{WO}_4/\text{SiO}_2$ powder catalyst was established at 3.95. This value is different to that reported in a previous work performed with the same catalyst powder in a single chamber configuration (0.85) [8]. It could be attributed to the double chamber reactor configuration used here, which improved the contact between methane and the oxygen electrochemically supplied. Finally, it is clear that the maximum C_{2+} yield was strongly higher for the Mn doped powder catalyst (16 vs. 10.4%), which would again demonstrate its better performance. It was achieved at a CH_4/O_2 ratio = 1.32. Hence, this catalytic system will be used in the following experiments focused on the use of natural gas.

3.3. Electro-catalytic experiments with natural gas

Even though methane is the main component of the natural gas, there are other hydrocarbons that could strongly affect the activity of the catalytic system. Hence, new experiments were carried out considering 1% natural gas (50 mL min^{-1} , N_2 balance) instead of methane as the outer chamber feed stream, and the SEC + PC system, accomplished with a bed of catalyst $\text{Mn}-\text{Ce}-\text{Na}_2\text{WO}_4/\text{SiO}_2$. The composition of the natural gas is given in Table 1. The feed stream of the inner chamber was the same as that used in the previous experiments (10% H_2O , 50 mL min^{-1} , N_2 balance). Fig. 7 shows the response of a dynamic galvanostatic transient experiment on the main reaction products obtained in the outer compartment, at a constant temperature of 800°C . The secondary axis of Fig. 7a depicts the theoretical H_2 produced at the inner chamber as a function of the Faraday's law, as previously explained in Fig. 3. Considering the composition of the natural gas, under open circuit potential conditions (OCV, current = 0 mA), a strong increase of the ethylene production rate was observed. In this sense, the outlet ethylene concentration under these conditions was similar to the inlet ethane concentration in the outer chamber feed stream. On the other hand, a strong increase of the hydrogen produced under OCV conditions was also observed. These results suggest that the main route for ethylene production was that of

the thermal cracking of ethane [24], since there is no oxygen electrochemically supplied to the outer chamber under OCV conditions. Moreover, the hydrogen production was higher than the corresponding to the above mentioned process, which could be attributed to the cracking or dehydrogenation of other hydrocarbons present in the natural gas. In addition, it is interesting to note that a small amount of CO_x was produced under OCV conditions, which would indicate that a slight spontaneous O_2 flux took place under these conditions. On the other hand, the application of currents from -10 to -60 mA led to a decrease of the hydrogen production respect the OCV conditions, with a progressive increase of the $\text{C}_{2\text{s}}$ and CO_x reaction rates, which could be again attributed to the enhancement of the kinetics corresponding to the methane oxidative coupling and partial or total combustion processes. Finally, Fig. 7 shows that the polarization effect was totally reversible, since the catalytic activity under the final OCV conditions were very similar to those considered at the beginning of the experiment.

The main parameters related to the catalytic activity of the SEC + PC system in the outer chamber were studied for the experiments described above. In addition, they were compared with the values obtained under similar reaction conditions with methane as the feed stream (Fig. 5). Fig. 8a depicts the ethylene yield variation with the applied current at 800°C . Firstly, a general increase of this parameter for both systems with the increase of the applied current can be observed. However, it seems that the system was more active toward ethylene production when natural gas was fed to the outer chamber. As previously mentioned, it could be attributed to the additional ethylene production from the heterogeneous/homogeneous oxidative dehydrogenation mechanism of the ethane present in the raw natural gas stream. On the other hand, the catalytic activity toward CO production is shown in Fig. 8b. Similarly to the trend observed in Fig. 8a, a general increase of this parameter was found when natural gas was fed to the outer chamber. The CO yield was around 1.5–2 times higher for the case of using natural gas than that for the case of using methane. It could be attributed to the partial oxidation of other hydrocarbons (apart from methane) with the O_2 supplied from the inner to the outer

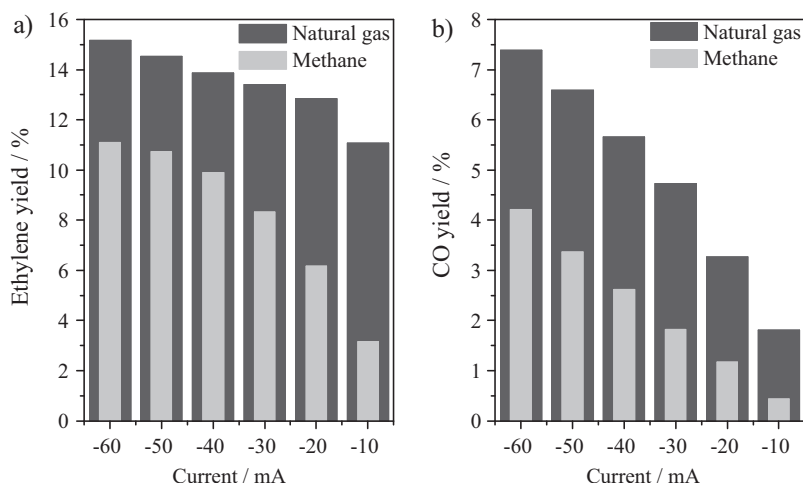


Fig. 8. Influence of the applied current on the steady state values of ethylene yield and CO yield of the outer chamber products for the Ag/YSZ/Ag+Mn-Ce-Na₂WO₄/SiO₂ system. Conditions: outer chamber natural gas = 1%, inner chamber H₂O = 10%, total flow in both chambers = 50 cm³ min⁻¹ (N₂ balance), temperature = 800 °C.

chamber by the steam electrolysis process since both, ethane and propane, are more reactive than methane [26].

Summarizing, the use of natural gas instead of methane is of interest for a practical development of this new technology. The configuration proposed in this study allowed to produce a pure hydrogen stream in the inner chamber by means of a steam electrolysis process. On the other hand, the oxygen electrochemically supplied from the inner chamber to the outer led to the production of C₂ hydrocarbons with high ethylene yields.

Taking into account the promising results obtained, a medium-term experiment was carried out for 24 h under the more severe conditions studied in this work, i.e., 800 °C and a constant current application of -60 mA. The main results (together with the H₂ production associated to the inner chamber steam electrolysis process) are shown in Fig. 9. A stable activity for the production of C₂s under these reaction conditions were observed, showing the stability of: the solid electrolyte, the Ag electrodes and the catalyst powder bed. It demonstrates a high potential for the practical development of the concept studied in this work.

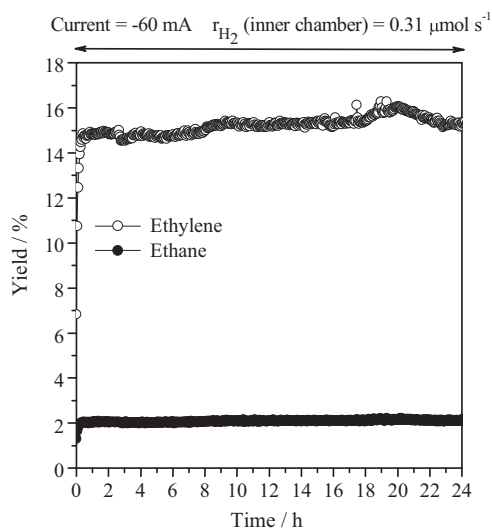


Fig. 9. Variation of C₂H₄ and C₂H₆ yields with the time on stream for the Ag/YSZ/Ag+Mn-Ce-Na₂WO₄/SiO₂ system. Conditions: outlet chamber Natural gas = 1%, inlet chamber H₂O = 10%, total flow in both chambers = 50 cm³ min⁻¹ (N₂ balance), temperature = 800 °C, current = -60 mA.

4. Conclusions

Several important findings can be obtained from this work:

- The new system developed in this study allowed to simultaneously produce and separate two important valuable products: H₂ and C₂ hydrocarbons.
- Reaction temperature and gas phase composition were optimized for two different catalyst powders (Ce-Na₂WO₄/SiO₂ and Mn-Ce-Na₂WO₄/SiO₂).
- The best performance was observed for the Mn doped catalyst. It was attributed to the higher crystallinity of this catalyst, together with a synergic effect between Mn, Na and W.
- Experiments with natural gas led to high ethylene yields in the outer chamber of the electro-catalytic system. Furthermore, a pure hydrogen production associated with the steam electrolysis process was located in the inner chamber.
- Durability tests demonstrated the high stability of the proposed system, which is quite important for its practical development.

Acknowledgements

We gratefully acknowledge Spanish MICINN projects CTQ 2007-62512/PPQ, CTQ 2008-02940-E (corresponding to ACENET ERA-NET project, ACE.07.016).

This work is also partially supported by projects PEst-C/eqb/LA0020/2011 and ACENET/0001/2007, financed by FEDER through COMPETE – Programa Operacional Factores de Competitividade and by FCT – Fundação para a Ciência e a Tecnologia. VJF gratefully acknowledges a PhD grant (SFRH/BD/33647/2009) by the Fundação para a Ciência e a Tecnologia (FCT).

References

- [1] Z. Gholipour, A. Malekzadeh, R. Hatami, Y. Mortazavi, A. Khodadadi, *Journal of Natural Gas Chemistry* 19 (2010) 35–42.
- [2] G.E. Keller, M.M. Bhasin, *Journal of Catalysis* 73 (1982) 9–19.
- [3] V. Kyriakou, C. Athanasiou, I. Garagounis, A. Skodra, M. Stoukides, *International Journal of Hydrogen Energy* 37 (2012) 16636–16641.
- [4] V. Kyriakou, C. Athanasiou, I. Garagounis, A. Skodra, M. Stoukides, *Solid State Ionics* 225 (2012) 219–222.
- [5] M. Stoukides, *Research on Chemical Intermediates* 32 (2006) 187–204.
- [6] M. Stoukides, *Catalysis Reviews – Science and Engineering* 42 (2000) 1–70.
- [7] A. Caravaca, A. de Lucas-Consuegra, J. González-Cobos, J.L. Valverde, F. Dorado, *Applied Catalysis B: Environmental* 113–114 (2012) 192–200.

- [8] A. Caravaca, V.J. Ferreira, A. de Lucas-Consuegra, J.L. Figueiredo, J.L. Faria, J.L. Valverde, F. Dorado, *International Journal of Hydrogen Energy* 38 (2013) 3111–3122.
- [9] S.M.K. Shahri, A.N. Pour, *Journal of Natural Gas Chemistry* 19 (2010) 47–53.
- [10] L. Wang, S. Tomura, F. Ohashi, M. Maeda, M. Suzuki, K. Inukai, *Journal of Materials Chemistry* 11 (2001) 1465–1468.
- [11] S. Ji, T. Xiao, S. Li, L. Chou, B. Zhang, C. Xu, R. Hou, A.P.E. York, M.L.H. Green, *Journal of Catalysis* 220 (2003) 47–56.
- [12] A. Trovarelli, *Catalysis by Ceria and Related Materials*, Imperial College Press, London, 2002.
- [13] S. Arndt, T. Otremba, U. Simon, M. Yildiz, H. Schubert, R. Schomäcker, *Applied Catalysis A: General* 425–426 (2012) 53–61.
- [14] X. Fang, S. Li, J. Lin, Y. Chu, F. Cuihua, *Journal of Molecular Catalysis* 6 (1992) 427–433.
- [15] S.-f. Ji, T.-c. Xiao, S.-b. Li, C.-z. Xu, R.-l. Hou, K.S. Coleman, M.L.H. Green, *Applied Catalysis A: General* 225 (2002) 271–284.
- [16] M.R. Lee, M.-j. Park, W. Jeon, J.-W. Choi, Y.-W. Suh, D.J. Suh, *Fuel Processing Technology* 96 (2012) 175–182.
- [17] T.P. Tiemersma, M.J. Tuinier, F. Gallucci, J.A.M. Kuipers, M.v.S. Annaland, *Applied Catalysis A: General* 433–434 (2012) 96–108.
- [18] P. Tsiakaras, C.G. Vayenas, *Journal of Catalysis* 144 (1993) 333–347.
- [19] Z. Cao, H. Jiang, H. Luo, S. Baumann, W.A. Meulenbergh, H. Voss, J. Caro, *Catalysis Today* 193 (2012) 2–7.
- [20] S. Ihara, *Bulletin of the Electrotechnical Laboratory, Tokyo* 41 (1977) 259–280.
- [21] J.O.M. Bockris, A.K.N. Reddy, M. Gamboa-Aldeco, *Modern Electrochemistry*, Kluwer Academic/Plenum, New York, 2000.
- [22] A. Palermo, J.P. Holgado Vazquez, A.F. Lee, M.S. Tikhov, R.M. Lambert, *Journal of Catalysis* 177 (1998) 259–266.
- [23] Z.-S. Chao, E. Ruckenstein, *Journal of Catalysis* 222 (2004) 17–31.
- [24] V.R. Choudhary, S.A.R. Mulla, *AIChE Journal* 43 (1997) 1545–1550.
- [25] S.A.R. Mulla, O.V. Buyevskaya, M. Baerns, *Applied Catalysis A: General* 226 (2002) 73–78.
- [26] O. Demoulin, B. Le Clef, M. Navez, P. Ruiz, *Applied Catalysis A: General* 344 (2008) 1–9.